Middle East oil and gas methane emissions signature captured at a remote site using light hydrocarbon tracers

Emeric Germain-Piaulenne, Jean-Daniel Paris, Valérie Gros, Pierre-Yves Quéhé, Michael Pikridas, Dominique Baisnée, Antoine Berchet, Jean Sciare, Efstratios Bourtsoukidis

ATMOSPHERIC ENVIRONMENT: X 22 (2024) 100253

Contents lists available at ScienceDirect

Atmospheric Environment: X

journal homepage: www.journals.elsevier.com/atmospheric-environment-x

Middle East oil and gas methane emissions signature captured at a remote site using light hydrocarbon tracers

Emeric Germain-Piaulenne [a,b], Jean-Daniel Paris [a,b,*], Valérie Gros [a], Pierre-Yves Quéhé [b], Michael Pikridas [b], Dominique Baisnée [a], Antoine Berchet [a], Jean Sciare [b], Efstratios Bourtsoukidis [b]

[a] Laboratoire des Sciences du Climat et de l'Environnement (LSCE), CEA-CNRS-UVSQ, IPSL, Gif sur Yvette, 91190, France
[b] Climate and Atmosphere Research Center, The Cyprus Institute (CyI), Nicosia, 2121, Cyprus

ARTICLE INFO

Keywords:
Methane
Non-methane hydrocarbons
Greenhouse gas emissions
Oil and gas emissions
Atmospheric observations
Emission inventories

ABSTRACT

The observational characterization of anthropogenic methane (CH_4) emissions in the Eastern Mediterranean and Middle East (EMME) region, known for its significant oil and gas (OG) production, remains limited. Light alkanes, such as ethane (C_2H_6), are co-emitted with CH_4 by OG activities and are promising tracers for identifying the CH_4 emissions from this sector at the wider regional scale. In this study, in-situ measurements of CH_4 and alkanes (C2–C8 were collected during a field campaign at a regional background site (Cape Greco, Cyprus). A mobile laboratory housed the instrumentation at the south-eastern edge of the island between December 2021 and February 2022. This specific location and time of year were selected to capture air masses originating from distant southern and eastern regions, primarily impacted by sources from the Middle East. Based on these observations we 1) evaluate the significance of long-range transported versus local sources in Cyprus, 2) identify and document regional anthropogenic CH_4 sources with the help of the concomitant alkane measurements, and 3) assess the accuracy of the EDGAR sectoral emission inventory over the EMME region. The highest alkane mixing ratios observed were associated with the Middle Eastern OG CH_4 signal. Surprisingly, the Middle Eastern emissions of CH_4 were found to be heavily influenced by the breeding and waste management sectors. By investigating the measured CH_4 mixing ratios together with an atmospheric dispersion model (FLEXPART), we derive a comprehensive characterization of the pollution sources at a regional scale over the Eastern Mediterranean region. Our results indicate that CH_4 emissions from the Middle Eastern OG sector are likely underestimated by ca. 69 %. These findings underscore the efficacy of using experimental observations of alkanes for CH_4 source identification at receptor sites. This tracer approach would also benefit from a substantial revision of light hydrocarbon emission inventories.

1. Introduction

Methane (CH_4) is the second most important anthropogenic greenhouse gas (GHG) after carbon dioxide (CO_2) (Saunois et al., 2020; IPCC, 2023) and responsible for 20–30 % of the global radiative forcing and thus the temperature increases since the pre-industrial era (Kirschke et al., 2013; EDGAR, 2022; IEA, 2023). More than half (50–65 %) of CH_4 emissions are anthropogenic. With its shorter lifetime compared to CO_2, CH_4 emission reduction offer important mitigation options in many sectors (Climate Change, 2022). Methane emissions remain underestimated in inventories, especially for the oil and gas (OG) sector (Schwietzke et al., 2016; Alvarez et al., 2018; Hmiel et al., 2020; Saunois et al., 2020; Zavala-Araiza et al., 2021; Paris et al., 2021; Stavropoulou et al., 2023). Current efforts to reduce uncertainties in regional OG emissions rely either on satellite measurements for large emitters or on intensive field campaigns that survey a limited number of sites with a high level of precision and sensitivity. Besides these dedicated efforts, the available long-term in situ CH_4 measurements contain information on regional OG emissions that remains underexploited because it cannot be simply attributed to the OG sector. Bourtsoukidis et al. (2019) and Paris et al. (2021) used co-emitted alkanes to attribute OG emission in ship campaign-based measurements of CH_4. This paper explores the possibility to expand this approach to fixed regional observatories.

Alkanes are a particular class of non-methane hydrocarbons

* Corresponding author. Laboratoire des Sciences du Climat et de l'Environnement (LSCE), CEA-CNRS-UVSQ, IPSL, Gif sur Yvette, 91190, France.
E-mail address: jean-daniel.paris@lsce.ipsl.fr (J.-D. Paris).

https://doi.org/10.1016/j.aeaoa.2024.100253
Received 18 October 2023; Received in revised form 28 February 2024; Accepted 23 March 2024
Available online 26 March 2024

(NMHCs) which are reactive trace gases that have numerous anthropogenic sources, including traffic, solvent use and OG activities. OG activities emit both CH_4 and alkanes in specific proportions that are representative of the source type. This can also be broken down to different levels of the value chain of the fossil fuel sector (Helmig et al., 2016; Bourtsoukidis et al., 2019; Paris et al., 2021). For example, natural gas (NG) contains more than 85 % CH_4 with a few percent of ethane, propane and other light alkanes with variations depending on the region and gas type (Burruss et al., 2014; Speight, 2018). Its composition evolves after extraction with condensation of heavier hydrocarbons and stripping of hydrogen sulfides. Fugitive emissions of NG, an important part of CH_4 anthropogenic emissions, will directly reflect its composition.

The atmospheric lifetimes of C2–C5 alkanes range from days to weeks, are compatible with atmospheric transport and are inversely proportional to their weight. The atmospheric ratio between C_2H_6 and CH_4 is used to determine the OG contribution of gas leaks in excess CH_4 found in urban or industrial environments (Defratyka et al., 2020; Fernandez et al., 2022) or even in large OG basins (Meyer et al., 2022). Close to the source, the value of this ratio is typically between 0.03 and 0.12 for NG fields. It can even reach 0.30 for emissions from oil fields or processed liquid NG (Xiao et al., 2008; Lopez et al., 2017; Yacovitch et al., 2020; Wilde et al., 2021). Lower ratios indicate atmospheric mixing with biogenic sources such as waste management or livestock farming that have typically zero C_2H_6 emission (Yacovitch et al., 2014; Assan et al., 2017). Despite its variability depending on the oil or gas field, the stage of the production line and the temperature of the gas (Yacovitch et al., 2020), this ratio provides indications for the identification of the OG-related emission sources. In the same lines, the ratio of pentane isomers (iso/n-pentane) has been frequently used for distinguishing OG sources, gasoline vapors and traffic emissions (Gilman et al., 2013; Bourtsoukidis et al., 2019; Paris et al., 2021). This ratio has been shown to be around 1 for raw NG emissions and is conserved during atmospheric transport. Higher ratios are reported in urban areas due to the lower n-pentane mixing ratio in processed gasoline caused by isomerization of petroleum after distillation, which aims to achieve a higher octane index (Paris et al., 2021).

The Middle East region, and especially the Arabian Gulf, hosts extensive OG operations (extraction, processing and storage). With almost half of the world's OG reserves, the production from this region is expected to increase over the next few decades (Khatib, 2014). An important number of super-emitters have recently been identified through satellite measurements with increasing spatial and magnitude resolution (Chen et al., 2023; Lauvaux et al., 2022). Efforts to gather in situ atmospheric measurements on CH_4 and related tracers in this region remain sparse. Paris et al. (2021) found that emissions in the Arabian Gulf were underestimated in the oil field areas (north) while they were slightly overestimated in the gas-dominated area (central Arabian Gulf). Al-Shalan et al. (2022) observed through ground-based mobile measurement that land emissions in Kuwait were dominated by waste management emissions instead of expected OG emissions.

The primary objective of this study is to investigate the potential of NMHCs in differentiating the OG component of CH_4 emissions at a regional scale, while concurrently evaluating the accuracy of sectoral emissions data provided by inventories. This study is based on a 3-month field campaign performed at a regional receptor site (Cyprus), with the aim to identify and characterize the sources of CH_4 at this site, with a specific focus on long-distance transport and the composition characteristics of NMHCs. To achieve this, we employ various analytical techniques, including source receptor modeling and back plume trajectories utilizing a Lagrangian particle dispersion model coupled with emission inventory data. By doing so, we seek to provide novel insights that either corroborate or challenge the existing inventory data on sectoral emissions.

2. Material and methods

2.1. Measurement site

A mobile laboratory was deployed between December 3rd, 2021 and February 24th, 2022 at the south-eastern edge of Cyprus, Cape Greco (34°57′41″ N, 34°04′55″ E and 17m above the mean sea level) (Fig. 1). Cape Greco is part of the municipality and seaside resort area of Ayia Napa. It is a national forest park primarily composed of low vegetation including shrubs and flowers.

Cyprus is a subtropical semi-arid Mediterranean climate island of 9251 km^2 and 1,2 M inhabitants. It is considered as a global warming hotspot (Zittis et al., 2015). It is situated in a climate sensitive region (EMME) with increasing temperatures, decreasing precipitation and degrading air quality (Lelieveld et al., 2016; Zittis et al., 2022). At a crossroad of atmospheric pollution from 3 continents (Lelieveld et al., 2002), it is well-positioned as a receptor site to study the long-range transport of GHGs and other atmospheric pollutants (Debevec et al., 2017). On a yearly basis (between 1997 and 2012), around 8 % of the airmasses originate from the Middle East, 11 % is of local/mixed origin, 22 % from north Africa and 59 % from Europe including Turkey and Russia (Kleanthous et al., 2014). A seasonal regional contribution has been derived from Lagrangian modelling performed at a background station at 532m above sea level between 1997 and 2015 showing a 10 % contribution from the Middle East, mainly during the winter period (Pikridas et al., 2018). During our observation period (December 2021–February 2022), around 21 % of the measured wind direction was East/South-East, 27 % was South/South-West and 52 % West/North (see Fig. 2 for data distribution according to wind direction).

2.2. Measurements

2.2.1. Greenhouse gases

We used a Picarro G2401 analyzer (Picarro) with a precision of 1 ppb for CH_4 that has been tested according to the ICOS-ATC protocol by continuous measurement repeatability (Kwok et al., 2015). The test showed good precision result (0.10 ppb per minute for CH_4) and good long-term repeatability (0.08 ppb for CH_4). The raw data acquired by the Picarro were processed (calibration corrections, filtering, water vapor correction) and quality-controlled on the ICOS (Integrated Carbon Observing System) Atmospheric thematic center database (Hazan et al., 2016). Laboratory-determined water vapor corrections in the data acquisition were applied before the campaign as described by Rella et al. (2013a), the maximum bias was of 0.10 ppb for CH_4.

Linear calibrations of 4 cycles of 30 min for each compound were performed on March 12, 2021 and January 28, 2022 using 3 cylinders of different concentrations (2233, 1916 and 2018 ppb for CH_4, 606, 105 and 190 ppb for CO, 422, 402 and 433 ppm for CO_2 respectively). These two calibrations sessions indicated good stability with a standard deviation for CH_4 lower than 0.8 ppb on the raw data. Quality control measures included daily injections of a WMO-scale-traceable target gas with known concentrations (2031 ppb, 161 ppb and 425 ppm for CH_4, CO and CO_2 respectively). For CH_4, the difference with the reference value is below 0.8 ppb during the whole campaign and the standard deviation is below 0.08 ppb when considering the minutes data.

2.2.2. Non-Methane Hydrocarbons

Two gas chromatographs coupled with Flame Ionization Detectors systems (airmoVOC and airmoBTX; Chromatotec - home, France) were used to monitor C2–C6 and C6–C12 hydrocarbons respectively. Both analyzers provide measurements every 30 min, the airmoVOC system employed a sampling time of 10 min with a flow rate of 11.6 mL min^{-1}, whereas the BTX (Benzene-Toluene-Xylene) system had a sampling time of 22.5 min with a flow rate of 43.5 mL min^{-1}. More details on the GCs can be found in Debevec et al. (2017) and Gros et al. (2011).

A gas cylinder containing a standard gas (NPL, Teddington,

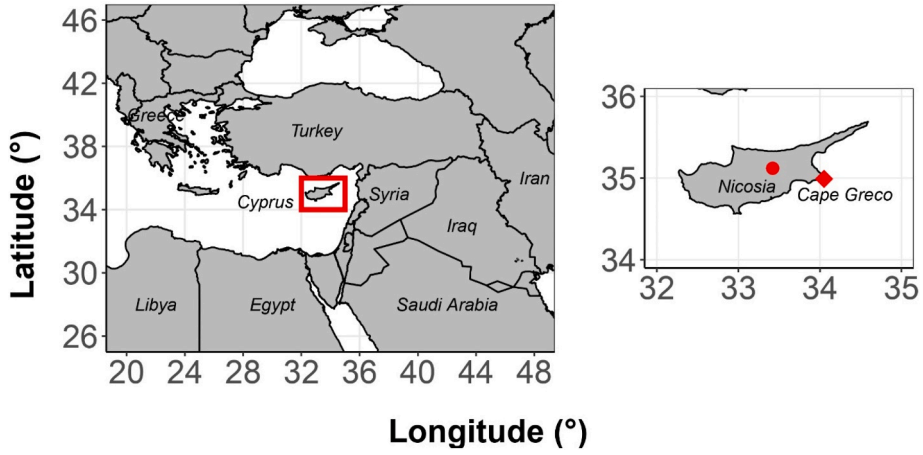

Fig. 1. Location of Cyprus in Eastern Mediterranean (left) and campaign site Cape Greco (right) compared to Cyprus' capital city Nicosia.

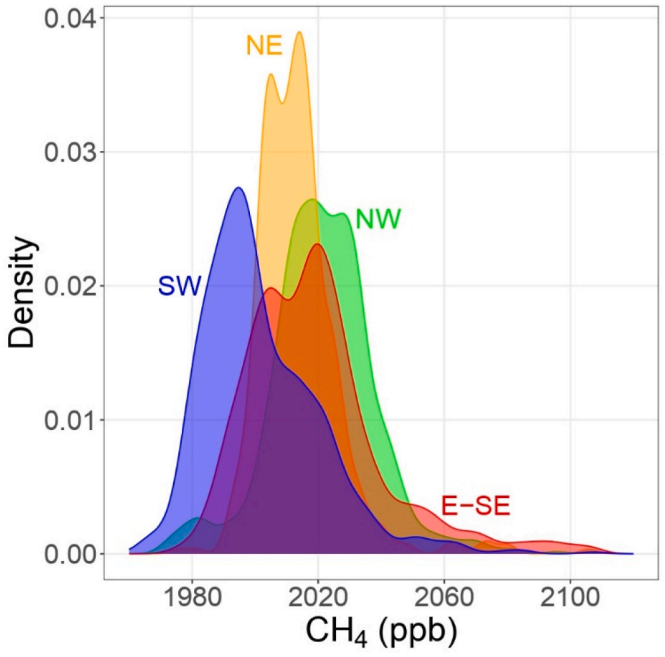

Fig. 2. Overview of observations with CH_4 mixing ratio data distribution according to wind direction (NW = 270-10°, NE = 10–50°, E-SE = 50–180°, SW = 180–270°).

Middlesex, UK) with approximately 4 ppb of each species was used for calibration purposes. Calibrations were performed on December 3rd, 2021 and January 28th, 2022. As all calibration coefficients stayed stable (within 8.7 % for the C2C6 compounds: 6.1 % for C_2H_6, 1.0 % for C_2H_4, 6.4 % for C_3H_8, 8.7 % for i-C_4H_{10}, 3.6 % for n-C_4H_{10}, 5.6 % for C_2H_2, 6.5 % for i-C_5H_{12} and 2.7% for n-C_5H_{12}) between both calibrations, a mean calibration coefficient was used for the whole campaign.

The detection limits (DL) varied according to the species, with values varying in a few parts per trillion (ppt) range (0.84 ppt for m&p-xylenes to 13.58 ppt for ethylene). More information on the detection limits and coefficients of standard variation by compound can be found in Table S1. The overall uncertainty of the C2–C12 hydrocarbon observations was calculated, taking into account factors such as calibration gas uncertainty, automatic processing, manual integration, and sensitivity to external conditions. The overall calculated uncertainty was determined to be approximately 10 ± 4 %, which is consistent with similar measurements conducted in previous studies (Debevec et al., 2017; Bourtsoukidis et al., 2019).

Due to technical issues with air compressor failure and power cuts, NMHCs C2 to C6 data are available from 03/12/2021 to 20/12/2021, 12/01/2022 to 18/01/2022 and 24/01/2022 to 24/02/2022 except 7th and 8th of February while C6 to C12 data are from 03/12/2021 to 20/12/2021 and 12/01/2022 to 18/01/2022.

2.3. Experimental setup

The analyzers were housed inside a mobile laboratory (van) and the air inlets were placed at the van roof level, 3 m above the ground (Fig. S1). A pump placed downstream of the instrumentation drew 200 ml min-1 of ambient air through a 4-m long stainless-steel sampling line (0.125 cm diameter). To prevent rainwater from entering the lines, a bell-shaped system was used. Additionally, a PTFE (polytetrafluoroethylene) filter with a nickel casing and a 1/4″ Swagelok connection was used to prevent dust from entering the analyzers. The temperature inside the mobile laboratory was constantly monitored and kept as constant as possible at 19 ± 4 °C to avoid thermal instability and ensure the proper operation of the instruments.

A geo-located mobile weather station was monitoring atmospheric pressure, temperature, wind speed and direction. A mean temperature of 14.1 ± 3.4 °C (range: 3.4 °C–22.8 °C) was measured during the campaign as well as wind speeds averaged 3.2 ± 2.1 m s^{-1} with 90 % of the time under 6 m s^{-1} according to our weather station. Mean relative humidity (68 ± 2 %), precipitation (21 ± 8 mm $month^{-1}$) and cloud cover (39 ± 2 % for the entire campaign period) data were obtained by the meteorological station of the nearby city of Ayia Napa, located at 8.2 km from the sampling site (Nomades, www.historique-meteo.net, last accessed: 03/08/23).

2.4. Lagrangian particle dispersion model simulation and inventories

The origin of the air masses at the receptor site was simulated using FLEXPART v10 (FLEXible PARTicle dispersion model), a Lagrangian model of atmospheric particle transport and dispersion (Seibert and Frank, 2004; Stohl et al., 2005; Pisso et al., 2019). In this study, 2000 particles per release every 3 h were followed 10 days backward in time and recorded at a 0.1° × 0.1° space resolution.

FLEXPART is driven by meteorological inputs data from the European Center for Medium-range Weather Forecast (ECMWF) ERA5 (Hittmeir et al., 2018) with a spatial resolution of 1° covering the northern hemisphere, 3-h intervals and 60 vertical layers. ECMWF data are retrieved and formatted using the FLEX-extract toolbox (Tipka et al., 2020). FLEXPART simulations were carried out within the GUI toolbox developed by Berchet et al. (2023).

The potential emission sensitivity (PES) is determined by the parti-

cle's residence time below 500m above ground-level over the previous 10 days. A sensitivity test was performed with 2000m threshold and showed minor variations (median difference <2 ppb). PES is then combined with the ground-level EDGAR v7 (Emission Database for Global Atmospheric Research) inventory to simulate a time series of CH_4 excess. EDGAR provides estimates for yearly CH_4 emissions and other species up to 2021 per sector of emissions (26 sectors including fuel exploitation, enteric fermentation, manure management solid waste landfills or waste water handling for example). The simulated increase in mixing ratios at receptor (C) from CH_4 flux in a given grid cell were calculated as:

$$C = \sum(x)\left[PES(x) * (Flux(x) * 1000) * \left(Mair / M\ CH_4\right)\right] \quad (4)$$

with PES expressed in ppb (g m^{-2} s^{-1})$^{-1}$, Flux from the EDGAR database in kg m^{-2} s^{-1}, and the air and CH_4 molar masses being respectively 28.97 and 16.04 g mol^{-1} and x being any gridcell.

We separated the simulated result by region of origin. The regions are defined as follows: Cyprus = 26 to 35°E, 34 to 36°N; Europe = −10 to 26°E, 34 to 60°N; Africa = −10 to 35°E, 10 to 34°N; Turkey = 26 to 43°E, 36 to 46°N; Middle East = 35 to 60°E, 10 to 36°N; Other = East and North of Turkey with Black and Caspian seas as well as East Europe and West Russia.

2.5. Source receptor Positive Matrix Factorization (PMF)

A NMHC source apportionment analysis using Positive Matrix Factorization (PMF) (Paatero, 1997) including 21 compounds has been performed for the period 4th to December 20, 2021, period when all NMHC data were available (see Suppl. A, Tables S2 and S3 for details on the simulation). We refer to Debevec et al. (2017); Pikridas et al. (2018) and Bourtsoukidis et al. (2020) for further PMF description and applications in EMME environments. PMF was applied to the native (30 min) resolution, using the EPA-PMF 5.0 software that implements the multilinear engine tool (ME-2; Paatero, 1997). A four-factor solution for this dataset was selected (see Suppl. A).

2.6. Definition of background mixing ratios

CH_4 and NMHCs will be analyzed as excess mixing ratios above the background levels, defined as:

$$\Delta X = [X] - [X]background \quad (5)$$

Where X is the species of interest. The background for the species X is defined as the average of the lowest 5th percentile of the measured mixing ratios within a 7-day time window at each measurement point. Fig. S2 provides further visual representation of this background calculation process.

3. Results

3.1. Atmospheric mixing ratios

The mean CH_4 mixing ratio at Cape Greco was 2011 ± 23 ppb during the campaign period. It exceeded the globally averaged marine surface monthly mean data from NOAA for the same period (1908 ppb). The mean background level was 1982 ± 11 ppb, with mean ΔCH_4 being at 30 ± 24 ppb. The CH_4 monthly mean (2009 ± 21 ppb) in December 2021 exceeded the monthly means at mid-latitude Northern Hemisphere background stations such as Terceira Island in Portugal (1970 ppb), Tudor Hill on Bermuda Island (1979 ppb), Mace Head in Ireland (1992 ppb) or Lampedusa in Italy (1997 ppb) (NOAA ESRL, https://gml.noaa.gov).

The monthly mean C_2H_6 mixing ratio observed at Cape Greco in December 2021 (2.07 ± 0.47 ppb) was also higher than the averaged marine surface monthly mean (1.67 ppb) provided by NOAA (NOAA ESRL, https://gml.noaa.gov). GHG and NMHC mixing ratio statistics in Cape Greco are summarized in Table S4.

Generally, CH_4 had positive correlation (r = 0.2–0.5) with light alkanes (C2 to C5) but also with other NMHCs (Table S5). Considering the entire dataset, C_2H_6 and CH_4 were moderately correlated ($r = 0.48$, $p < 10^{-15}$). The Pearson correlation between ΔCH_4 and ΔCO_2 and ΔCH_4 and ΔCO was around 0.7 and 0.8 respectively. This suggests that a mixture of sources including combustion sources as well as some influence from thermogenic emissions influenced our measurements over the observation period.

Fig. 2 shows CH_4 distribution for different wind sectors. The highest CH_4 mixing ratios (up to 2127 ppb) were observed under E-SE wind directions (see also Fig. S3). Wind speeds of more than 4 m s^{-1} dominated in this sector, compatible with long-range advection of air masses. When air masses passed above the island ("NW direction" in Fig. 2), high CH_4 mixing ratios (mean = 2022 ± 17 ppb) were observed. These may be due to local Cypriot sources, with agriculture and waste sectors likely playing a prominent role (Liu, 2022). Lower mixing ratios (2002 ± 19 ppb) are observed with SW wind direction (Mediterranean Sea), showing the absence of major nearby sources in this sector (Fig. 2).

3.2. Regional and sector contributions: simulated CH_4 and indications from light alkanes

Over the 3-month campaign, the mean simulated CH_4 excess was 27 ± 18 ppb, overall in good agreement with the observed mean of the 3-h ΔCH_4 (29 ± 22 ppb). Over the 3-month campaign, measured and simulated total ΔCH_4 are loosely correlated ($r = 0.17$, $p = 1.8*10^{-5}$). The variability of simulated ΔCH_4 was 18 ppb, close to the measured ΔCH_4 std dev (22 ppb). Simulated enhancements are overall considered as a satisfactory representation of the measurements and warrant the analysis of simulated enhancements decomposed by sectors and regions.

Enteric fermentation and solid waste landfills contributed 27 % each to the simulated signal at the receptor site. Fuel exploitation (gas, oil and coal fugitive emissions according to the IPCC AR6 WGIII guidelines for national greenhouse gas inventories) contributed 21 %, followed by waste water handling at 13 %, manure management at 7 %. 14 other sectors account for the remaining 5 %.

We identified 16 events, defined as elevated CH_4 mixing ratios combined with contiguous period with a dominant region contribution being at a maximum >75 %. Each of these events, was attributed to a single region of origin (i.e. Cyprus, Europe, Africa, Turkey origin and Middle East). Europe and Cyprus were dominated by enteric fermentation (4 out of 5 events). All 4 Turkey origin events were dominated by landfills emissions. Fuel exploitation dominated 6 out of 7 events from Africa and Middle East.

Alkanes data were available during 11 out of the 16 events. The lowest ΔC_2H_6: ΔCH_4 ratio (0.014) and highest i/n-C_5H_{12} ratio (1.12) measured ratio were identified for European events (Fig. 3), which is consistent with the dominance of biogenic sources and urban centers influence in Europe (Yacovitch et al., 2014; Bourtsoukidis et al., 2019). Comparably low ratios were calculated for African and Turkish events with respectively 0.021 and 0.025 for ΔC_2H_6: ΔCH_4 ratio and 0.84 and 0.85 for i/n-C_5H_{12} ratio (Fig. 3).

The highest ΔC_2H_6: ΔCH_4 ratios (0.058) were calculated for Middle East events. During these events, a unit i/n-C_5H_{12} ratio (1.00) was found. These measured ratios are consistent with a strong OG signature in CH_4 originating from the Middle East.

3.3. Synoptic case studies on Middle east and Eastern Mediterranean emissions

We now focus (Fig. 4) on the December period as contrasted events of different geographical and sectorial origins were observed during this period. Measured and simulated ΔCH_4 are reasonably well correlated ($r = 0.38$, $p = 3.5*10^{-6}$) between the 4th and 21st of December ($r = 0.58$,

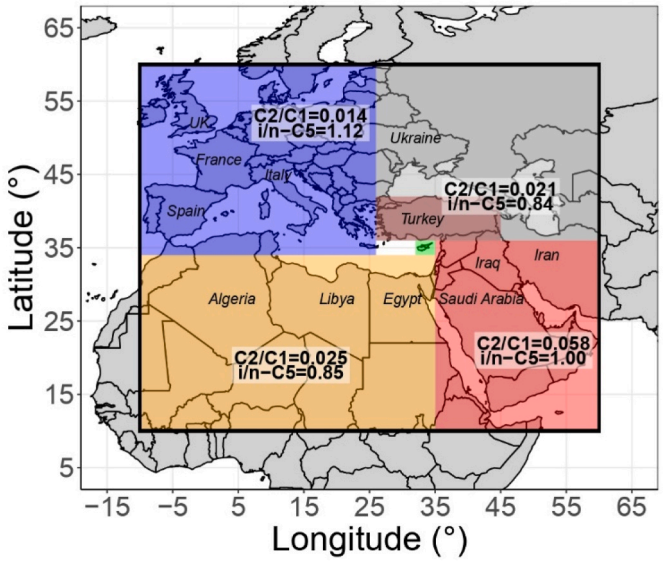

Fig. 3. Regional partition and respective median ΔC_2H_6: ΔCH_4 (C2/C1) and i/n-C_5H_{12} (i/n-C5).

$p = 2.4*10^{-13}$ when punctual anti-correlation periods due to model failure, see section 4.1, are not taken into account). Total simulated excess of CH_4 compared to observed enhancements can be found in Fig. S4.

Between 11th and 19th December, 2 advection events combined CH_4 enhancements and a clear dominant regional origin occurred consecutively (Fig. 4), one with an airmass from Middle East (hereafter referred to as "ME") and one from Turkey and Europe ("TE").

We define the ME event as the period from the 11 to 14th of December, with a maximum CH_4 on 14th December. During this entire period the PES is largely centered over the Middle East (with 62% of the PES on average residing over the Middle East region, this proportion increasing up to 85 % toward the end of the period and the maximum CH_4).

The TE event occurred from the 16th to 19th of December and is defined by a PES progressively positioned over Turkey and north of Turkey region, labeled "Other" on Fig. 4 (combined mean of 50 % up to 90 %). The ME and TE events are analyzed in the two following subsections.

3.3.1. *Relationship between CH_4 and alkanes in the Middle East event*

During the ME event, fuel exploitation represents up to 43% of simulated mean excess CH_4 (from 18 % on December 12th-00h UTC to 43 % on the 14th-00h UTC, mean 26%). The other sectors contributing to mean ΔCH_4 are enteric fermentation (25 %), solid waste landfills (21 %) and wastewater handling (18 %) (Fig. 4).

Fig. 5 shows the variability of trace gases mixing ratios during the ME event. The ME event exhibited a mean CH_4 of 2017 ± 19 ppb and 2.20 ± 0.58 ppb of C_2H_6. The highest C_2H_6 mixing ratios of the campaign were observed during this event, reaching a maximum value of 4.51 ppb while CH_4 enhancement was 31 ppb. Other light alkane (C3 to C5) mixing ratios were also very high during this period compared to the rest of the campaign, with no correlation with CO_2 or CO signals, pointing at a regional co-emitting source(s) of CH_4 and light alkanes alone, pointing to OG activities. The absence of alkenes on the first part of the ME event can be due to their absence in the emitting sources or their reaction during the long-range transport.

At the very end of the ME event (on December 14th), there was an observed increase of compounds emitted by combustion including C_2H_4, C_2H_2, ΔCO_2 and ΔCO along with ΔCH_4 (reaching up to 75 ppb). This suggests the additional influence of a combustion source located closer to the receptor site because of the relatively short lifetime of ethene, which is approximately one day. This increase in combustion-related compounds coincides with the "tail" of ME event's air mass, which is particularly sensitive to emissions originating from the Middle East. However, this increase is also associated with a PES more localized on the eastern part of the Mediterranean coast before going back to Europe. This is slightly different from the rest of the event where PES is more spread across the Arabian Peninsula (see Fig. 4 and Figs. S3 and S5).

Fig. 6 displays the relationship between C_2H_6 and CH_4 for different

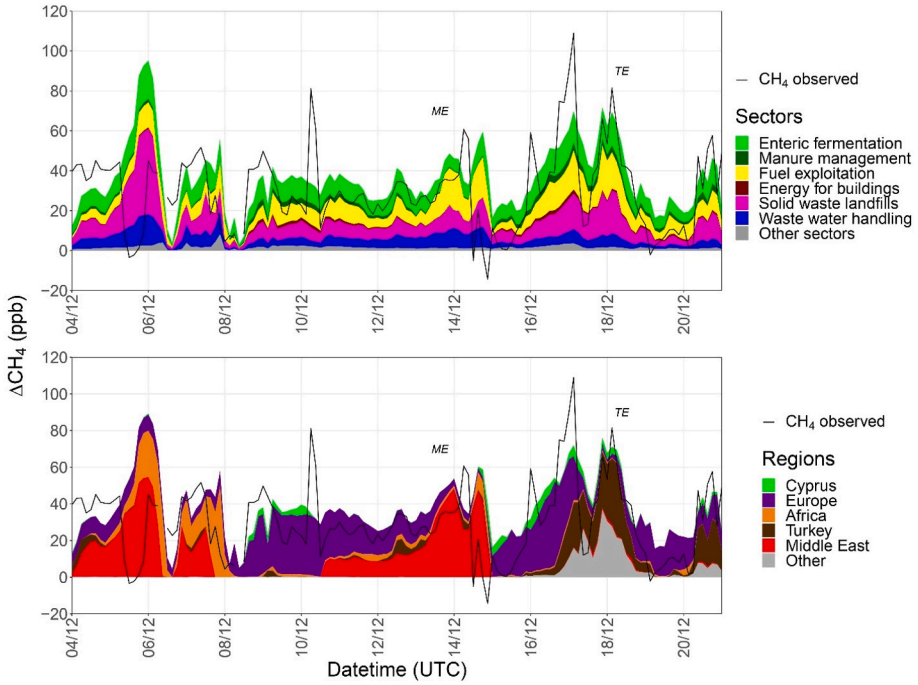

Fig. 4. Simulated ΔCH_4 decomposed by sector (top) and geographical region (bottom) for December 2021. The "ME" label indicate the Middle East event and "TE" the Turkey/Europe event.

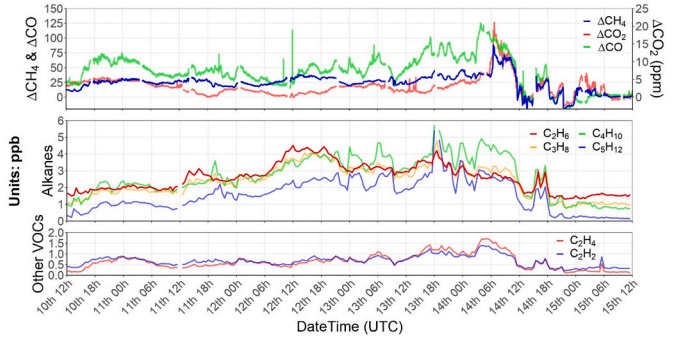

Fig. 5. Timeseries of enhancements of CH_4, CO_2, CO, C_2H_6, C_3H_8, C_4H_{10}, C_5H_{12}, C_2H_4, C_2H_2, during the ME event period.

wind sectors, highlighting a distinct correlation during the ME event in contrast to the entire dataset. This subset of data with airmasses originating from East and South-East directions, exhibits a clearer and statistically significant correlation between the two species ($r = 0.58$, $p < 10^{-15}$, see Table S6) and has a regression slope of approximately 7 % (0.069 ppb ppb^{-1}). This is consistent with the emission ratio reported for the Arabian Gulf region (0.062 ppb ppb^{-1}) during the AQABA ship campaign in 2017 (Paris et al., 2021). This suggests that the regional signal can be preserved during long-range transport.

In contrast to the ME event, when the wind originated from the West (NW and SW, which include local sources from Cyprus), the mixing ratios of C_2H_6 and CH_4 were distributed around a slope of 0.01 ppb ppb^{-1} (Fig. 6). These contrasted observations indicate that the OG emissions from the Middle East dominate CH_4 enhancements during the ME event, with very limited mixing with air poorer in C_2H_6.

Fig. 7 shows the observed i/n-C_5H_{12} ratios during the ME event (between December 11 and 14th), compared to the rest of the period. During the ME event it exhibits a distinct linear relationship between isomers with a stable ratio at 1.0 ± 0.2. This ratio is identified as typical of raw NG. Raw NG is NG prior to commercial gas processing, either

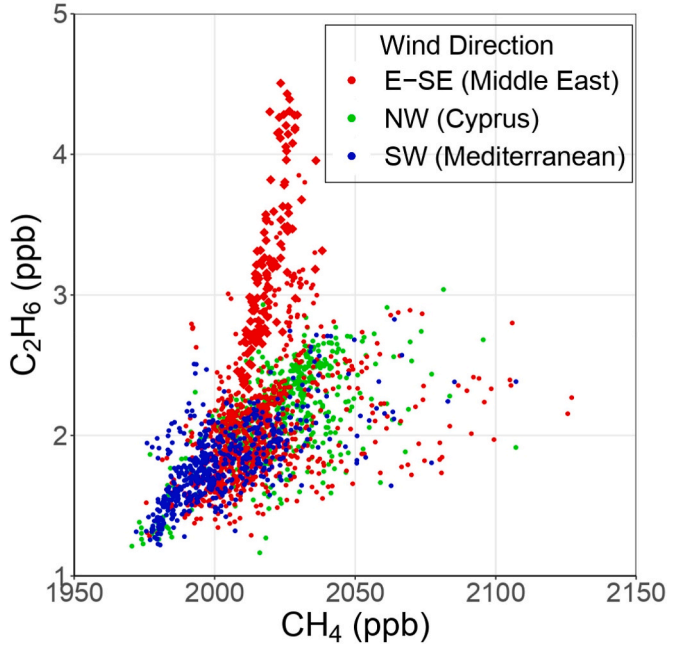

Fig. 6. C_2H_6 versus CH_4 mixing ratios (in ppb) clustered for different wind direction bins that were defined as: NW (Cyprus) for 270°–15°, E-SE (Middle East region) for 15°–180° and SW (Mediterranean) for 180°–270°. All points available during the 3-month campaign are displayed with the ME event being highlighted in larger diamond shape.

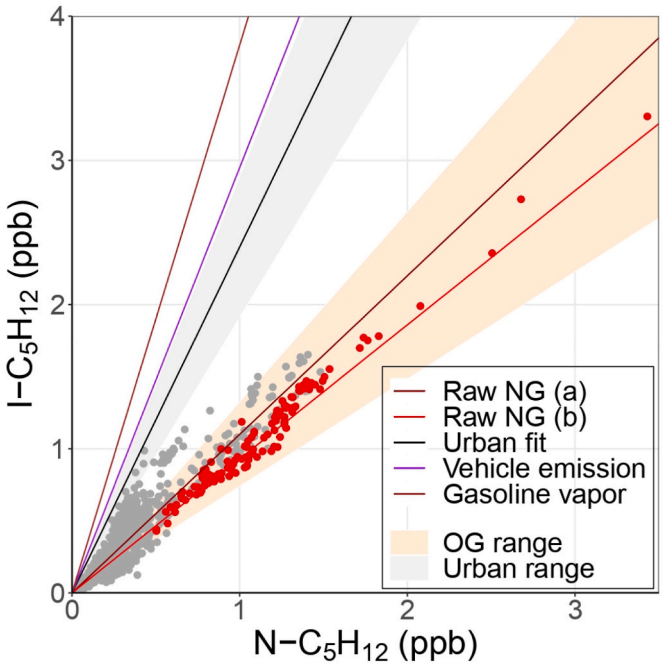

Fig. 7. Relationships between pentane isomers with red points corresponding to the ME event. Raw NG (b), Urban fit, Vehicle emission and Gasoline vapor lines used in Bourtsoukidis et al. (2019) and Raw NG (a) line from Wilde et al. (2021). NG and Urban ranges are ±20 % of corresponding lines. Reference lines are described in Broderick and Marnane (2002); Baker et al. (2008); Gentner et al. (2009); Gilman et al. (2013); Wilde et al. (2021). (For interpretation of the references to colour in this figure legend, the reader is referred to the Web version of this article.)

fugitive from oil wells or as leaked product from gas fields extraction. Raw NG emissions corresponds, in the IPCC Guidelines for National Greenhouse Gas Inventories 2019 revision to energy fugitive emissions subcategories 1B2aii (oil production), 1B2bii (NG production) and 1B2iii (NG processing). The ratio suggests that CH_4 OG emissions from the ME are strongly dominated by these upstream fugitive CH_4 emissions.

Combined with the ΔC_2H_6: ΔCH_4 slope of 7 %, this suggests a dominant influence of the OG sector (especially raw NG, the upstream step of the NG activity chain) in the emissions during the ME event. This strongly suggests that the OG emissions during this event are largely related to NG, upstream in the production chain.

Results from NMHC PMF performed on the December dataset were used in order to quantitatively exploit the signature of co-emitted NMHCs with CH_4 during the ME event. From the four factors identified by the PMF (see Suppl. A and Fig. S6), two of them correlated with CH_4 during the ME event (Fig. S7). The first factor, associated exclusively with light alkanes (C2 to C8), but not with other NMHC (alkenes, aromatics), positively correlates with CH_4 enhancement ($r = 0.66$ with $p < 10^{-15}$) during the ME event. This factor (with $r^2 = 0.44$) thus explains 44 % of observed CH_4 variance (between the 11th noon and 14th midnight). This value is a conservative estimate since the correlation ranges between 43% and 59 % when discarding the first hours of the ME event to test the sensitivity to the event definition.

The weight of light alkanes in this factor is consistent with emissions from OG upstream fugitive emissions, indicating that 44% (range: 43–59 %) of CH_4 emissions come from OG upstream sector in this event. The higher contribution of C_3H_8 (19 %) in this first factor compare to C_2H_6 (11 %) tend to show a significant impact of the oil sector more than raw NG in which we expect more C_2H_6 than C_3H_8 (Bourtsoukidis et al., 2019).

The second factor is characterized by heavier compounds (including

benzene, toluene and aromatics) and correlates, even if weakly, with ΔCH_4 ($r = 0.40$ with $p = 7.10^{-6}$) during the ME event (between December 11 and 14th). This factor also explains a non-negligible fraction of CH_4 variance (16 %). This last factor might be linked to maritime traffic and/or east Mediterranean coast oil refineries because it is also associated with alkenes and strongly correlates with CO ($r = 0.87$ with $p < 10^{-15}$), an external combustion marker (see Table S7 for detailed correlation coefficients between PMF factors and greenhouse gases). This further suggests that our quantitative attribution of nearly half of the CH_4 excess during the ME event to the middle-eastern OG upstream sector, derived from the first factor might be a conservative estimate. A higher fraction of OG from the middle east would also be compatible with our data. This discrepancy may be due to the fact that incomplete combustion and leaks downstream from the production chain, with different NMHC signatures, are not properly considered.

3.3.2. The European and Turkish event

A distinct event occurred between the 16th and the 19th December, with maxima ΔCH_4 reaching up to 109 and 81 ppb (during night-time on the 17th and the 18th respectively, hereafter "TE"). The simulated sectoral contribution is very similar to the ME event with 26 % for fuel exploitation, 26 % for enteric fermentation, 25 % for solid waste landfills and 10 % for wastewater handling during this second event (Fig. 4). However, the FLEXPART footprint indicates a clearly different origin than the ME event, with an influence on airmass sensitivity shifting to Europe and Turkey (Fig. 4). This different geographical and therefore sectoral origin is also clearly seen on the alkane's signatures. A median ΔC_2H_6: ΔCH_4 ratio of 0.005 ± 0.001 was observed on the 16th when air masses came in majority from Europe. The ratio then changed to 0.020 ± 0.001 on the 17th with footprint shifting to Turkey. This northern airmass is most likely also influenced by Eastern Europe and Western Russia signal (included in the "Other" contribution in Fig. 4). Additionally, the median i/n-C_5H_{12} ratio was 1.33 ± 0.31 (1.72 ± 0.22 on the 16th and 1.40 ± 0.12 on the 17th). These ratio differ (lower and higher respectively for ΔC_2H_6: ΔCH_4 and i/n-C_5H_{12} ratios) from the signatures in these ratio derived during the ME and point to sources different from OG activities. For airmasses influenced by Turkey, we found a higher correlation between CH_4 and C_2H_2 (0.76 instead of 0.60 over the entire period of December), as well as with C_2H_4 (0.59 instead of 0.48), which are short-lived compounds (Parrish et al., 2007) and combustion markers which could be related to coal activities (Dudzińska, 2014). Since no wild fires was reported close to the measurement site or on the trajectories of the airmasses (EFFIS, https://effis.jrc.ec.europa.eu/, last accessed: 07/08/23) at this specific period (11 to December 19, 2021), we have cautiously excluded the possible influence of biomass burning. The examination of these markers and footprints shows that coal operations in Western Turkey (less than 2 days transport of the air masses) may have significantly contributed to the observed signal. This would be consistent with the Global Carbon Budget reports (Friedlingstein et al., 2022) that highlight the importance of the coal sector in this country. Further isotopic data for $\delta^{13}CH_4$ observations would be useful in this region during this type of events to identify biomass burning and coal mining influence.

4. Discussions

4.1. Modelling uncertainties

Many uncertainties remain in our simulations, both in the Lagrangian model or the inventory used. For example, the relative proximity of local sources at scales comparable to model spatial resolution can lead to strong errors due to improper positioning of sources or poor mixing representation.

The irregularity and ephemeral nature of certain emissions like flaring or venting is also a factor that can explain the mismatch between observation and simulations. These can also be explained by the fact that the inventory has no variability and is static within a year, meaning that daily, weekly or even seasonally, emission variations are not considered and won't be reproduced by the model.

Punctual strong anti-correlation between observed and total simulated (on the 5th and 14th December especially) can be explained by transport model failure in the timing of regime change with errors in wind fields associated to drop in atmospheric pressure and strong change in the potential emission sensitivity. We confirmed this hypothesis of poor model performances by looking at the pressure data from the meteorological station which highlight the low-pressure drops during these failures.

Despite these uncertainties, the relatively good correlation found between simulated and observed CH_4 during the ME event allows to further investigate this event.

4.2. OG contribution during ME event

77 % of Middle East emissions come from OG (without the coal sector) according to EDGAR v7.0 emission inventory. With our coarse regional definition, the inventory predicts a contribution of 74 % of OG in the Middle East region.

During the ME event the mean contribution of the OG sector is 26 % (maximum 43%). This fraction based on EDGAR and the PES takes into account coal mining and handling production, upgrading and transport of OG as well as venting and flaring of NG.

We consider factors that may play on the different OG proportion simulated during the ME event (26–43%) and the general inventory. First, the seasonality emissions from the OG sector, it is low, seems to peak between October and March (Chen et al., 2018), December not being in the maximum months (Javadinejad et al., 2019). Therefore, it likely does not play a significant role here.

Then, the PES is not evenly distributed across all Middle East countries. During the ME event, simulations show a higher sensitivity (higher PES) to emissions from Syria, Lebanon, Jordan, Iraq and Saudi Arabia than for other Middle East countries. For these countries, EDGAR estimates a 75 % ratio of OG emissions, therefore ensuring representativity of the regional Middle East mean.

The PES also encompass Europe, Turkey and Africa; these regions exhibit significantly different fraction of predicted OG emissions depending on the region (Table S8). This explains most of the dilution of the share of OG emission in DCH_4 between the regional inventory and the simulated ME event.

Finally, the proportion of PES sensitive to Middle East during the ME event was variable and this induces a varying sensitivity to ME OG emissions. The fraction of Middle Eastern contribution to CH_4 enhancement varies during the ME event from 34 % to 92 % (Fig. 4), the maximum being during the evening on the 13th. Over this event the OG over total simulated ratio varies from 18 to 43 % (around the mean of 26 %). The maxima of both OG and ME coincide, on December 14th at midnight (see back-plume trajectories on Fig. S5).

4.3. Implications for inventories

As demonstrated in section 3.3.1, the light alkanes analysis indicates that Middle eastern OG upstream sector is the dominant sector explaining CH_4 enhancements during the ME event. The simulation is broadly consistent with the light alkane results, and this can be put in the perspective of the high numbers of super-emitters recently identified in this region (Lauvaux et al., 2022; Chen et al., 2023). The similarity of the ΔC_2H_6: ΔCH_4 ratio during the ME event with the one measured in the Arabian Gulf suggest that OG had a much larger share than simulated during the ME event. The PMF provided indication that OG upstream and midstream sectors explain 43–59 % of CH_4 during the event, much more than the 24–31 % predicted by our simulation. The i/n-C_5H_{12} ratio gives more specific information within the OG sector and points to a dominant contribution of upstream raw NG while the PMF first factor

point to oil sector contribution. Our result points to a likely underestimation of 69 % (plausible range 48–146 % - this uncertainty range being obtained by varying the time window used) of the OG Middle East emissions in the inventory.

CH_4 emissions from Europe, Turkey and the Middle East, with their distinct sectoral mixes, have different light alkane signatures (Fig. 3). During the TE event, the ΔC_2H_6: ΔCH_4 ratio is higher under Turkey's influence than under Europe's influence. Symmetrically, the i/n-C_5H_{12} ratio is lower with Turkey's contribution than under dominant Europe/Cyprus sensitivity. This suggests that the airmasses coming from Europe/Cyprus are affected by a comparatively more important mixed urban signature than Turkey. The broader fossil fuel sector, including coal (due to enhanced C_2H_2 especially during the TE event) as well as OG from farther away in the north and/or east, appears to influence significantly airmasses passing over Turkey.

In this study, we show that the CH_4 emissions coming from the OG sector in the EDGAR database seems underestimated in the Middle East region. This is consistent with recent studies (Guha et al., 2020; Foulds et al., 2022; Liu, 2022; Yu et al., 2023) that have shown that OG but also the landfill sector might be underestimated in inventory of CH_4 emissions. With different methods, Dalsøren et al. (2016); Maasakkers et al. (2019); Al-Shalan et al. (2022) or Lauvaux et al. (2022) point also in the direction of an underestimation OG CH_4 emission as well as the waste sector in the Middle East region.

Local CH_4 emissions in Cyprus, even if underestimated in the inventories (Liu, 2022), are primarily dominated by agricultural and waste-related activities (EDGARv7.0), specifically concentrated in the central part of the island. In our Lagrangian modeling, the emissions from sources such as cattle farms (with enteric fermentation) and waste management (with landfills), were the biggest contributors to the simulated CH_4 signal during this 3-month campaign. However, the FLEXPART configuration used here was aimed at studying regional signal and do not offer the sufficient spatial and temporal resolution to analyze in depth Cypriot national emissions.

The EDGAR v7 NMHC emissions inventory data significantly underestimate the atmospheric levels of light hydrocarbons and has not been updated for over ten years (EDGAR last sectoral and global speciated NMHCs emission files are for the year 2012 in v4). This prevents their effective use in the backward simulation modelling and thus, calculate an accurate expected C_2H_6 on CH_4 ratio coming from specific region or sectors to improve CH_4 estimation and being able to effectively quantify their contribution on observed CH_4 signal. Moreover, there is a possibility that atmospheric chemistry-based projections of methane abundance could be underestimated due to the extended atmospheric lifetimes resulting from the inaccurate simulation of NMHCs.

5. Conclusions

Measurements of greenhouse gasses and light hydrocarbons, were carried out over a three-month period at the southeastern coast of Cyprus. The campaign aimed to address pollution transport from regional sources that affect CH_4 abundance in the eastern Mediterranean and to investigate the feasibility of analysing regional Middle Eastern signatures from a remote background receptor site. A comparison of the observed data with model simulations demonstrated that while CH_4 is reasonably well represented in the model, emissions from the OG sector in the Middle East are underestimated.

Utilizing light alkane ratios, especially ΔC_2H_6: ΔCH_4 and i/n-C_5H_{12}, as well as PMF, this study showed the OG sector's regional influence on the CH_4 mixing ratios. A distinct event in mid-December 2021 was observed coming from the Middle East and was specifically studied with enhancement relationships. The ΔC_2H_6: ΔCH_4 ratio strongly indicates the predominant contribution of the OG sector from this region while the i-/n-pentane ratio indicates influence by NG activities on top of other sources and especially upstream NG. Despite being about 2000 km away from the Arabian Gulf, light alkane measurements enable the identification of a preserved signal, distinguishing CH_4 OG emission sector from other sources despite the dilution and long-range transport processes in place at regional scale.

Simulated CH_4 mixing ratios are dominated by enteric fermentation (27 %), solid waste disposal landfills (27 %) and fuel exploitation (21 %). The PMF light alkanes signature points to a likely underestimation of 69 % (48–146 %) of the OG contribution in the inventory. Therefore, it appears that a large part of the emissions is related to fugitive emissions from the OG sector. It's noteworthy that in conjuction with fugitive oil emission and other energy sectors, these fugitive OG emissions are reported to have large substantial uncertainties (50–200 %) in the EDGAR inventory (Solazzo et al., 2021).

The regional signature, characterized by ΔC_2H_6: ΔCH_4 and i/n-C_5H_{12} ratios, was deducted by combining light alkane measurements with simulations. This allowed us to distinctly discern the variations in emission structures across sectors clearly between Europe, Turkey and Middle East with urban dominance, coal contribution and OG influence respectively.

Our study highlights the value of monitoring atmospheric CH_4 in conjunction with NMHC at receptor sites. The inclusion of NMHCs in source characterization, whether through hydrocarbon ratios or PMF analyses, can serve as a valuable addition to FLEXPART model simulations. The methodology of integrating measurements and modelling for CH_4 and NMHCs can be applied on other existing or planned monitoring sites that measure both CH_4 and NMHC.

CRediT authorship contribution statement

Emeric Germain-Piaulenne: Data curation, Formal analysis, Investigation, Methodology, Resources, Software, Validation, Visualization, Writing – original draft, Writing – review & editing. **Jean-Daniel Paris:** Conceptualization, Formal analysis, Funding acquisition, Methodology, Project administration, Resources, Supervision, Validation, Writing – review & editing, Investigation. **Valérie Gros:** Conceptualization, Formal analysis, Funding acquisition, Methodology, Project administration, Resources, Supervision, Validation, Writing – review & editing, Investigation. **Pierre-Yves Quéhé:** Data curation, Methodology. **Michael Pikridas:** Investigation, Methodology, Software. **Dominique Baisnée:** Methodology, Software. **Antoine Berchet:** Methodology, Software. **Jean Sciare:** Conceptualization, Formal analysis, Funding acquisition, Project administration, Resources, Supervision, Validation, Writing – review & editing. **Efstratios Bourtsoukidis:** Conceptualization, Formal analysis, Funding acquisition, Investigation, Methodology, Project administration, Resources, Supervision, Validation, Writing – review & editing.

Declaration of competing interest

The authors declare that they have no known competing financial interests or personal relationships that could have appeared to influence the work reported in this paper.

Data availability

The datasets are open access available at https://doi.org/10.5281/zenodo.10007536. The codes and data are available upon request to all scientists.

Acknowledgments

This work was supported by the European Union's Horizon 2020 research and innovation program [grant No. 856612] and the Cyprus Government (EMME-CARE). We further acknowledge the support from the project "ACCEPT" (Prot. No: LOCALDEV-0008) which financed by the Financial Mechanism of Norway. We extend our gratitude to the Department of Forests of the Republic of Cyprus for granting us access to

Cape Greco location, which enabled us to conduct the measurements for this study.

Appendix A. Supplementary data

Supplementary data to this article can be found online at https://doi.org/10.1016/j.aeaoa.2024.100253.

References

Al-Shalan, A., Lowry, D., Fisher, R.E., Nisbet, E.G., Zazzeri, G., Al-Sarawi, M., France, J. L., 2022. Methane emissions in Kuwait : plume identification, isotopic characterisation and inventory verification. Atmos. Environ. 268, 118763 https://doi.org/10.1016/j.atmosenv.2021.118763.

Alvarez, R.A., Zavala-Araiza, D., Lyon, D.R., Allen, D.T., Barkley, Z.R., Brandt, A.R., Davis, K.J., Herndon, S.C., Jacob, D.J., Karion, A., Kort, E.A., Lamb, B.K., Lauvaux, T., Maasakkers, J.D., Marchese, A.J., Omara, M., Pacala, S.W., Peischl, J., Robinson, A.L., Hamburg, S.P., 2018. Assessment of methane emissions from the U.S. oil and gas supply chain. Science. https://doi.org/10.1126/science.aar7204 eaar7204.

Assan, S., Baudic, A., Guemri, A., Ciais, P., Gros, V., Vogel, F.R., 2017. Characterization of interferences to in situ observations of δ13 CH_4 and C_2H_6 when using a cavity ring-down spectrometer at industrial sites. Atmos. Meas. Tech. 10 (6), 2077–2091. https://doi.org/10.5194/amt-10-2077-2017.

Baker, A.K., Beyersdorf, A.J., Doezema, L.A., Katzenstein, A., Meinardi, S., Simpson, I.J., Blake, D.R., Sherwood Rowland, F., 2008. Measurements of nonmethane hydrocarbons in 28 United States cities. Atmos. Environ. 42 (1), 170–182. https://doi.org/10.1016/j.atmosenv.2007.09.007.

Berchet, A., Pison, I., Narbaud, C., 2023. FLEXPART-GUI-toolbox. Zenodo. https://doi.org/10.5281/zenodo.7766372.

Bourtsoukidis, E., Ernle, L., Crowley, J.N., Lelieveld, J., Paris, J.D., Pozzer, A., Walter, D., Williams, J., 2019. Non-methane hydrocarbon (C2–C8) sources and sinks around the Arabian Peninsula. Atmos. Chem. Phys. 19 (10), 7209–7232. https://doi.org/10.5194/acp-19-7209-2019.

Bourtsoukidis, E., Pozzer, A., Sattler, T., Matthaios, V.N., Ernle, L., Edtbauer, A., Fischer, H., Könemann, T., Osipov, S., Paris, J.D., Pfannerstill, E.Y., Stönner, C., Tadic, I., Walter, D., Wang, N., Lelieveld, J., Williams, J., 2020. The Red Sea Deep Water is a potent source of atmospheric ethane and propane. Nat. Commun. 11 (1) https://doi.org/10.1038/s41467-020-14375-0.

Broderick, B.M., Marnane, I.S., 2002. A comparison of the C2–C9 hydrocarbon compositions of vehicle fuels and urban air in Dublin, Ireland. Atmos. Environ. 36 (6), 975–986. https://doi.org/10.1016/s1352-2310(01)00472-1.

Burruss, R.C., Ryder, R.T., 2014. Composition of natural gas and crude oil produced from 14 wells in the Lower Silurian "Clinton" Sandstone and Medina Group Sandstones, northeastern Ohio and northwestern Pennsylvania. In: Ruppert, L.F., Ryder, R.T. (Eds.), Coal and Petroleum Resources in the Appalachian Basin; Distribution, Geologic Framework, and Geochemical Character. U.S. Geological Survey Professional Paper 1708, p. 38. https://doi.org/10.3133/pp1708G.6 chap. G.6 of.

Chen, Z., Griffis, T.J., Baker, J.M., Millet, D.B., Wood, J.D., Dlugokencky, E.J., Andrews, A.E., Sweeney, C., Hu, C., Kolka, R.K., 2018. Source partitioning of methane emissions and its seasonality in the U.S. Midwest. J. Geophys. Res. : Biogeosciences 123 (2), 646–659. https://doi.org/10.1002/2017jg004356.

Chen, Z., Jacob, D.J., Gautam, R., Omara, M., Stavins, R.N., Stowe, R.C., Nesser, H.O., Sulprizio, M.P., Lorente, A., Varon, D.J., Lu, X., Shen, L., Qu, Z., Pendergrass, D.C., Hancock, S., 2023. Satellite quantification of methane emissions and oil/gas methane intensities from individual countries in the Middle East and North Africa: implications for climate action. EGUsphere. https://doi.org/10.5194/egusphere-2022-1504 [preprint].

Chromatotec - home. Retrieved September 1st, 2023, from. http://www.chromatotec.com/ANALYSEUR,GAZ-Home-18.html?lang=en.

Climate Change, 2022. In: Shukla, P.R., Skea, J., Slade, R., Al Khourdajie, A., van Diemen, R., McCollum, D., Pathak, M., Some, S., Vyas, P., Fradera, R., Belkacemi, M., Hasija, A., Lisboa, G., Luz, S., Malley, J. (Eds.), Mitigation of Climate Change. Contribution of Working Group III to the Sixth Assessment Report of the Intergovernmental Panel on Climate Change. Cambridge University Press, Cambridge, UK and New York, NY, USA. https://doi.org/10.1017/9781009157926.001.

Dalsøren, S.B., Myhre, C.L., Myhre, G., Gomez-Pelaez, A.J., Søvde, O.A., Isaksen, I.S.A., Weiss, R.F., Harth, C.M., 2016. Atmospheric methane evolution the last 40 years. Atmos. Chem. Phys. 16 (5), 3099–3126. https://doi.org/10.5194/acp-16-3099-2016.

Debevec, C., Sauvage, S., Gros, V., Sciare, J., Pikridas, M., Stavroulas, I., Salameh, T., Leonardis, T., Gaudion, V., Depelchin, L., Fronval, I., Sarda-Esteve, R., Baisnée, D., Bonsang, B., Savvides, C., Vrekoussis, M., Locoge, N., 2017. Origin and variability in volatile organic compounds observed at an Eastern Mediterranean background site (Cyprus). Atmos. Chem. Phys. 17 (18), 11355–11388. https://doi.org/10.5194/acp-17-11355-2017.

Defratyka, S.M., Paris, J.D., Yver-Kwok, C., Loeb, D., France, J., Helmore, J., Yarrow, N., Gros, V., Bousquet, P., 2020. Ethane measurement by Picarro CRDS G2201-i in laboratory and field conditions: potential and limitations. Atmos. Meas. Tech. 14 (7), 5049–5069. https://doi.org/10.5194/amt-14-5049-2021.

Dudzińska, A., 2014. Investigation of adsorption and desorption of acetylene on hard coal samples from Polish mines. Int. J. Coal Geol. 128-129, 24–31. https://doi.org/10.1016/j.coal.2014.03.007.

EDGAR, 2022. (Emissions Database for Global Atmospheric Research) Community GHG Database (A Collaboration between the European Commission, Joint Research Centre (JRC), the International Energy Agency (IEA), and Comprising IEA-EDGAR CO2, EDGAR CH4, EDGAR N2O, EDGAR F-GASES Version 7.0. European Commission, JRC (Datasets). Retrieved September 1st, 2023, from. https://edgar.jrc.ec.europa.eu/dataset_ghg70.

EFFIS - Welcome to EFFIS. (s. d.). Retrieved September 1st, 2023, from https://effis.jrc.ec.europa.eu/.

Fernandez, J.M., Maazallahi, H., France, J.L., Menoud, M., Corbu, M., Ardelean, M., Calcan, A., Townsend-Small, A., van der Veen, C., Fisher, R.E., Lowry, D., Nisbet, E. G., Röckmann, T., 2022. Street-level methane emissions of Bucharest, Romania and the dominance of urban wastewater. Atmos. Environ. X 13, 100153. https://doi.org/10.1016/j.aeaoa.2022.100153.

Foulds, A., Allen, G., Shaw, J.T., Bateson, P., Barker, P.A., Huang, L., Pitt, J.R., Lee, J.D., Wilde, S.E., Dominutti, P., Purvis, R.M., Lowry, D., France, J.L., Fisher, R.E., Fiehn, A., Pühl, M., Bauguitte, S.J.B., Conley, S.A., Smith, M.L., et al., 2022. Quantification and assessment of methane emissions from offshore oil and gas facilities on the Norwegian continental shelf. Atmos. Chem. Phys. 22 (7), 4303–4322. https://doi.org/10.5194/acp-22-4303-2022.

Friedlingstein, P., O'Sullivan, M., Jones, M.W., Andrew, R.M., Gregor, L., Hauck, J., Le Quéré, C., Luijkx, I.T., Olsen, A., Peters, G.P., Peters, W., Pongratz, J., Schwingshackl, C., Sitch, S., Canadell, J.G., Ciais, P., Jackson, R.B., Alin, S.R., Alkama, R., et al., 2022. Global carbon budget 2022. Earth Syst. Sci. Data 14 (11), 4811–4900. https://doi.org/10.5194/essd-14-4811-2022.

Gentner, D.R., Harley, R.A., Miller, A.M., Goldstein, A.H., 2009. Diurnal and seasonal variability of gasoline-related volatile organic compound emissions in riverside, California. Environ. Sci. Technol. 43 (12), 4247–4252. https://doi.org/10.1021/es9006228.

Gilman, J.B., Lerner, B.M., Kuster, W.C., de Gouw, J.A., 2013. Source signature of volatile organic compounds from oil and natural gas operations in northeastern Colorado. Environ. Sci. Technol. 47 (3), 1297–1305. https://doi.org/10.1021/es304119a.

Gros, V., Gaimoz, C., Herrmann, F., Custer, T., Williams, J., Bonsang, B., Sauvage, S., Locoge, N., d'Argouges, O., Sarda-Estève, R., Sciare, J., 2011. Volatile organic compounds sources in Paris in spring 2007. Part I : qualitative analysis. Environ. Chem. 8 (1), 74. https://doi.org/10.1071/en10068.

Guha, A., Newman, S., Fairley, D., Dinh, T.M., Duca, L., Conley, S.C., Smith, M.L., Thorpe, A.K., Duren, R.M., Cusworth, D.H., Foster, K.T., Fischer, M.L., Jeong, S., Yesiller, N., Hanson, J.L., Martien, P.T., 2020. Assessment of regional methane emission inventories through airborne quantification in the San Francisco bay area. Environ. Sci. Technol. 54 (15), 9254–9264. https://doi.org/10.1021/acs.est.0c01212.

Hazan, L., Tarniewicz, J., Ramonet, M., Laurent, O., Abbaris, A., 2016. Automatic processing of atmospheric CO_2 and CH_4 mixing ratios atthe ICOS Atmosphere Thematic Centre. Atmos. Meas. Tech. 9 (9), 4719–4736. https://doi.org/10.5194/amt-9-4719-2016.

Helmig, D., Rossabi, S., Hueber, J., Tans, P., Montzka, S.A., Masarie, K., Thoning, K., Plass-Duelmer, C., Claude, A., Carpenter, L.J., Lewis, A.C., Punjabi, S., Reimann, S., Vollmer, M.K., Steinbrecher, R., Hannigan, J.W., Emmons, L.K., Mahieu, E., Franco, B., Pozzer, A., 2016. Reversal of global atmospheric ethane and propane trends largely due to US oil and natural gas production. Nat. Geosci. 9 (7), 490–495. https://doi.org/10.1038/ngeo2721.

Hittmeir, S., Philipp, A., Seibert, P., 2018. A conservative reconstruction scheme for the interpolation of extensive quantities in the Lagrangian particle dispersion model FLEXPART. Geosci. Model Dev. (GMD) 11 (6), 2503–2523. https://doi.org/10.5194/gmd-11-2503-2018.

Hmiel, B., Petrenko, V.V., Dyonisius, M.N., Buizert, C., Smith, A.M., Place, P.F., Harth, C., Beaudette, R., Hua, Q., Yang, B., Vimont, I., Michel, S.E., Severinghaus, J.P., Etheridge, D., Bromley, T., Schmitt, J., Faïn, X., Weiss, R.F., Dlugokencky, E., 2020. Preindustrial 14 CH_4 indicates greater anthropogenic fossil CH_4 emissions. Nature 578 (7795), 409–412. https://doi.org/10.1038/s41586-020-1991-8.

IEA, 2023. Global Methane Tracker 2023. IEA, Paris. https://www.iea.org/reports/global-methane-tracker-2023. License: CC BY 4.0.

IPCC, 2023. Summary for policymakers. In: Lee, H., Romero, J. (Eds.), Climate Change 2023: Synthesis Report. Contribution of Working Groups I, II and III to the Sixth Assessment Report of the Intergovernmental Panel on Climate Change [Core Writing Team. IPCC, Geneva, Switzerland, pp. 1–34. https://doi.org/10.59327/IPCC/AR6-9789291691647.001.

Javadinejad, S., Eslamian, S., Ostad-Ali-Askari, K., 2019. Investigation of monthly and seasonal changes of methane gas with respect to climate change using satellite data. Appl. Water Sci. 9 (8) https://doi.org/10.1007/s13201-019-1067-9.

Khatib, H., 2014. Oil and natural gas prospects: Middle East and North Africa. Energy Pol. 64, 71–77. https://doi.org/10.1016/j.enpol.2013.07.091.

Kirschke, S., Bousquet, P., Ciais, P., Saunois, M., Canadell, J.G., Dlugokencky, E.J., Bergamaschi, P., Bergmann, D., Blake, D.R., Bruhwiler, L., Cameron-Smith, P., Castaldi, S., Chevallier, F., Feng, L., Fraser, A., Heimann, M., Hodson, E.L., Houweling, S., Josse, B., Zeng, G., 2013. Three decades of global methane sources and sinks. Nat. Geosci. 6 (10), 813–823. https://doi.org/10.1038/ngeo1955.

Kleanthous, S., Vrekoussis, M., Mihalopoulos, N., Kalabokas, P., Lelieveld, J., 2014. On the temporal and spatial variation of ozone in Cyprus. Sci. Total Environ. 476-477, 677–687. https://doi.org/10.1016/j.scitotenv.2013.12.101.

Kwok, Y.C., Laurent, O., Guemri, A., Philippon, C., Wastine, B., Rella, C.W., Vuillemin, C., Truong, F., Delmotte, M., Kazan, V., Darding, M., Lebègue, B.,

Kaiser, C., Xueref-Rémy, I., Ramonet, M., 2015. Comprehensive laboratory and field testing of cavity ring-down spectroscopy analyzers measuring H20, C02, CH_4 and CO. Atmos. Meas. Tech. 8 (9), 3867–3892. https://doi.org/10.5194/amt-8-3867-2015.

Lauvaux, T., Giron, C., Mazzolini, M., d'Aspremont, A., Duren, R., Cusworth, D., Shindell, D., Ciais, P., 2022. Global assessment of oil and gas methane ultra-emitters. Science 375 (6580), 557–561. https://doi.org/10.1126/science.abj4351.

Lelieveld, J., Berresheim, H., Borrmann, S., Crutzen, P.J., Dentener, F.J., Fischer, H., Feichter, J., Flatau, P.J., Heland, J., Holzinger, R., Korrmann, R., Lawrence, M.G., Levin, Z., Markowicz, K.M., Mihalopoulos, N., Minikin, A., Ramanathan, V., de Reus, M., Roelofs, G.J., Ziereis, H., 2002. Global air pollution crossroads over the mediterranean. Science 298 (5594), 794–799. https://doi.org/10.1126/science.1075457.

Lelieveld, J., Proestos, Y., Hadjinicolaou, P., Tanarhte, M., Tyrlis, E., Zittis, G., 2016. Strongly increasing heat extremes in the Middle East and North Africa (MENA) in the 21st century. Climatic Change 137 (1–2), 245–260. https://doi.org/10.1007/s10584-016-1665-6.

Liu, Y., 2022. Characterizing Methane (CH4) and Carbon Dioxide (CO2) Emissions through Mobile Platforms from Local to National Scale. Global Changes. Université Paris-Saclay; The Cyprus Institute. English. ⟨NNT : 2022UPASJ021⟩. ⟨tel-03974255⟩.

Lopez, M., Sherwood, O.A., Dlugokencky, E.J., Kessler, R., Giroux, L., Worthy, D.E.J., 2017. Isotopic signatures of anthropogenic CH4 sources in Alberta, Canada. Atmos. Environ. 164, 280–288. https://doi.org/10.1016/j.atmosenv.2017.06.021.

Maasakkers, J.D., Jacob, D.J., Sulprizio, M.P., Scarpelli, T.R., Nesser, H., Sheng, J.X., Zhang, Y., Hersher, M., Bloom, A.A., Bowman, K.W., Worden, J.R., Janssens-Maenhout, G., Parker, R.J., 2019. Global distribution of methane emissions, emission trends, and OH concentrations and trends inferred from an inversion of GOSAT satellite data for 2010–2015. Atmos. Chem. Phys. 19 (11), 7859–7881. https://doi.org/10.5194/acp-19-7859-2019.

Meyer, A.G., Lindenmaier, R., Heerah, S., Benedict, K.B., Kort, E.A., Peischl, J., Dubey, M.K., 2022. Using multiscale ethane/methane observations to attribute coal mine vent emissions in the san juan basin from 2013 to 2021. J. Geophys. Res. Atmos. 127 (18) https://doi.org/10.1029/2022jd037092.

NOAA ESRL. Global monitoring laboratory. Retrieved September 1st, 2023, from. https://gml.noaa.gov/.

Nomades, D.C.. Historique-Météo.net. Historique Météo. Retrieved September 1st, 2023, from. https://www.historique-meteo.net/.

Paatero, P., 1997. Least squares formulation of robust non-negative factor analysis. Chemometr. Intell. Lab. Syst. 37 (1), 23–35. https://doi.org/10.1016/s0169-7439(96)00044-5.

Paris, J.-D., Riandet, A., Bourtsoukidis, E., Delmotte, M., Berchet, A., Williams, J., Ernle, L., Tadic, I., Harder, H., Lelieveld, J., 2021. Shipborne measurements of methane and carbon dioxide in the Middle East and Mediterranean areas and the contribution from oil and gas emissions. Atmos. Chem. Phys. 21 (16), 12443–12462. https://doi.org/10.5194/acp-21-12443-2021.

Parrish, D.D., Stohl, A., Forster, C., Atlas, E.L., Blake, D.R., Goldan, P.D., Kuster, W.C., de Gouw, J.A., 2007. Effects of mixing on evolution of hydrocarbon ratios in the troposphere. J. Geophys. Res. Atmos. 112 (D10) https://doi.org/10.1029/2006jd007583.

Pikridas, M., Vrekoussis, M., Sciare, J., Kleanthous, S., Vasiliadou, E., Kizas, C., Savvides, C., Mihalopoulos, N., 2018. Spatial and temporal (short and long-term) variability of submicron, fine and sub-10 μm particulate matter (PM1, PM2.5, PM10) in Cyprus. Atmos. Environ. 191, 79–93. https://doi.org/10.1016/j.atmosenv.2018.07.048.

Picarro | Continuous monitoring for real time insights. Retrieved September 1st, 2023, from https://www.picarro.com/.

Pisso, I., Sollum, E., Grythe, H., Kristiansen, N.I., Cassiani, M., Eckhardt, S., Arnold, D., Morton, D., Thompson, R.L., Groot Zwaaftink, C.D., Evangeliou, N., Sodemann, H., Haimberger, L., Henne, S., Brunner, D., Burkhart, J.F., Fouilloux, A., Brioude, J., Philipp, A., Stohl, A., 2019. The Lagrangian particle dispersion model FLEXPART version 10.4. Geosci. Model Dev. (GMD) 12 (12), 4955–4997. https://doi.org/10.5194/gmd-12-4955-2019.

Rella, C.W., Chen, H., Andrews, A.E., Filges, A., Gerbig, C., Hatakka, J., Karion, A., Miles, N.L., Richardson, S.J., Steinbacher, M., Sweeney, C., Wastine, B., Zellweger, C., 2013a. High accuracy measurements of dry mixing ratios of carbon dioxide and methane in humid air. Atmos. Meas. Tech. 6 (3), 837–860. https://doi.org/10.5194/amt-6-837-2013.

Saunois, M., Stavert, A.R., Poulter, B., Bousquet, P., Canadell, J.G., Jackson, R.B., Raymond, P.A., Dlugokencky, E.J., Houweling, S., Patra, P.K., Ciais, P., Arora, V.K., Bastviken, D., Bergamaschi, P., Blake, D.R., Brailsford, G., Bruhwiler, L., Carlson, K. M., Carrol, M., Zhuang, Q., 2020. The global methane budget 2000–2017. Earth Syst. Sci. Data 12 (3), 1561–1623. https://doi.org/10.5194/essd-12-1561-2020.

Schwietzke, S., Sherwood, O.A., Bruhwiler, L.M.P., Miller, J.B., Etiope, G., Dlugokencky, E.J., Michel, S.E., Arling, V.A., Vaughn, B.H., White, J.W.C., Tans, P. P., 2016. Upward revision of global fossil fuel methane emissions based on isotope database. Nature 538 (7623), 88–91. https://doi.org/10.1038/nature19797.

Seibert, P., Frank, A., 2004. Source-receptor matrix calculation with a Lagrangian particle dispersion model in backward mode. Atmos. Chem. Phys. 4 (1), 51–63. https://doi.org/10.5194/acp-4-51-2004.

Solazzo, E., Crippa, M., Guizzardi, D., Muntean, M., Choulga, M., Janssens-Maenhout, G., 2021. Uncertainties in the emissions database for global atmospheric research (EDGAR) emission inventory of greenhouse gases. Atmos. Chem. Phys. 21 (7), 5655–5683. https://doi.org/10.5194/acp-21-5655-2021.

Speight, J.G., 2018. Natural Gas : A Basic Handbook. Elsevier Science & Technology Books.

Stavropoulou, F., Vinković, K., Kers, B., de Vries, M., van Heuven, S., Korbeń, P., Schmidt, M., Wietzel, J., Jagoda, P., Necki, J.M., Bartyzel, J., Maazallahi, H., Menoud, M., van der Veen, C., Walter, S., Tuzson, B., Ravelid, J., Morales, R.P., Emmenegger, L., Brunner, D., Steiner, M., Hensen, A., Velzeboer, I., van den Bulk, P., Denier van der Gon, H., Delre, A., Edjabou, M.E., Scheutz, C., Corbu, M., Iancu, S., Moaca, D., Scarlat, A., Tudor, A., Vizireanu, I., Calcan, A., Ardelean, M., Ghemulet, S., Pana, A., Constantinescu, A., Cusa, L., Nica, A., Baciu, C., Pop, C., Radovici, A., Mereuta, A., Stefanie, H., Hermans, B., Schwietzke, S., Zavala-Araiza, D., Chen, H., Röckmann, T., 2023. High potential for CH4 emission mitigation from oil infrastructure in one of EU's major production regions. EGUsphere. https://doi.org/10.5194/egusphere-2023-247 [preprint].

Stohl, A., Forster, C., Frank, A., Seibert, P., Wotawa, G., 2005. Technical note: the Lagrangian particle dispersion model FLEXPART version 6.2. Atmos. Chem. Phys. 5 (9), 2461–2474. https://doi.org/10.5194/acp-5-2461-2005.

Tipka, A., Haimberger, L., Seibert, P., 2020. Flex_extract v7.1.2 – a software package to retrieve and prepare ECMWF data for use in FLEXPART. Geosci. Model Dev. (GMD) 13 (11), 5277–5310. https://doi.org/10.5194/gmd-13-5277-2020.

Wilde, S.E., Dominutti, P.A., Allen, G., Andrews, S.J., Bateson, P., Bauguitte, S.J.B., Burton, R.R., Colfescu, I., France, J., Hopkins, J.R., Huang, L., Jones, A.E., Lachlan-Cope, T., Lee, J.D., Lewis, A.C., Mobbs, S.D., Weiss, A., Young, S., Purvis, R.M., 2021. Speciation of VOC emissions related to offshore North Sea oil and gas production. Atmos. Chem. Phys. 21 (5), 3741–3762. https://doi.org/10.5194/acp-21-3741-2021.

Xiao, Y., Logan, J.A., Jacob, D.J., Hudman, R.C., Yantosca, R., Blake, D.R., 2008. Global budget of ethane and regional constraints on U.S. sources. J. Geophys. Res. 113 (D21) https://doi.org/10.1029/2007jd009415.

Yacovitch, T.I., Herndon, S.C., Roscioli, J.R., Floerchinger, C., McGovern, R.M., Agnese, M., Pétron, G., Kofler, J., Sweeney, C., Karion, A., Conley, S.A., Kort, E.A., Nähle, L., Fischer, M., Hildebrandt, L., Koeth, J., McManus, J.B., Nelson, D.D., Zahniser, M.S., Kolb, C.E., 2014. Demonstration of an ethane spectrometer for methane source identification. Environ. Sci. Technol. 48 (14), 8028–8034. https://doi.org/10.1021/es501475q.

Yacovitch, T.I., Daube, C., Herndon, S.C., 2020. Methane emissions from offshore oil and gas platforms in the Gulf of Mexico. Environ. Sci. Technol. 54 (6), 3530–3538. https://doi.org/10.1021/acs.est.9b07148.

Yu, X., Millet, D.B., Henze, D.K., Turner, A.J., Delgado, A.L., Bloom, A.A., Sheng, J., 2023. A high-resolution satellite-based map of global methane emissions reveals missing wetland, fossil fuel, and monsoon sources. Atmos. Chem. Phys. 23 (5), 3325–3346. https://doi.org/10.5194/acp-23-3325-2023.

Zavala-Araiza, D., Omara, M., Gautam, R., Smith, M.L., Pandey, S., Aben, I., Almanza-Veloz, V., Conley, S., Houweling, S., Kort, E.A., Maasakkers, J.D., Molina, L.T., Pusuluri, A., Scarpelli, T., Schwietzke, S., Shen, L., Zavala, M., Hamburg, S.P., 2021. A tale of two regions: methane emissions from oil and gas production in offshore/onshore Mexico. Environ. Res. Lett. 16 (2), 024019 https://doi.org/10.1088/1748-9326/abceeb.

Zittis, G., Hadjinicolaou, P., Fnais, M., Lelieveld, J., 2015. Projected changes in heat wave characteristics in the eastern Mediterranean and the Middle East. Reg. Environ. Change 16 (7), 1863–1876. https://doi.org/10.1007/s10113-014-0753-2.

Zittis, G., Almazroui, M., Alpert, P., Ciais, P., Cramer, W., Dahdal, Y., Fnais, M., Francis, D., Hadjinicolaou, P., Howari, F., Jrrar, A., Kaskaoutis, D.G., Kulmala, M., Lazoglou, G., Mihalopoulos, N., Lin, X., Rudich, Y., Sciare, J., Stenchikov, G., et al., 2022. Climate change and weather extremes in the Eastern Mediterranean and Middle East. Rev. Geophys. https://doi.org/10.1029/2021rg000762.